Supporting Information

Traaseth et al. 10.1073/pnas.0904290106

Materials and Methods

Sample Preparation. [U-^{15}N] AFA-PLN was expressed in *Escherichia coli* bacteria and purified as described (1). Most of the selectively labeled samples were also expressed in *E. coli*. PLN samples that showed isotopic scrambling, [^{15}N-Ser] and [^{15}N-Gln], were synthesized using Fmoc solid-phase peptide synthesis as reported previously (2, 3). The composition of each peptide was verified by amino acid analysis and its molecular mass was verified by MALDI-TOF. For solution NMR experiment, AFA-PLN was solubilized in 300 mM DPC, 120 mM NaCl, 20 mM NaH_2PO_4 (pH 6.0). Solid-state NMR samples were prepared in either 4/1 DOPC/DOPE or DOPC lipid bilayers as previously described (no difference in spectra was discernable with or without DOPE) (4). Lipids (80 mg) were dissolved in 4 ml chloroform (Avanti Polar Lipids) and added to PLN (≈4 mg) that was first solubilized in 100 μl trifluoroethanol. Solvents were first evaporated under a stream of N_2 (g) and then placed in a vacuum desiccator overnight to ensure complete removal of organic solvents. The lipid/protein film was resuspended in 40 ml of H_2O and vortexed. Small unilamellar vesicles were prepared by extruding the lipid mixture through polycarbonate filters of decreasing pore size (200, 100, 50 μm) using a bench-top extruder (Northern Lipids Inc. Burnaby, BC Canada). This suspension was concentrated to 2 ml in volume and placed evenly onto ≈25 glass plates (Marienfeld, 5.7 mm × 12 mm × 80 μm). Samples were hydrated for 4–5 days at 40 °C in a saturated solution of Na_2HPO_4. The [U-^{15}N] AFA-PLN sample was hydrated in a saturated solution of Na_2HPO_4 in D_2O. Solid-state NMR data were acquired at 30 °C.

NMR Spectroscopy. Solution NMR resonance assignments, NOEs, and ^3J-coupling constants were collected under conditions of 300 mM DPC (pH 6) and at 37 °C. For solid-state NMR, 2D PISEMA (5) and SAMPI4 (6) experiments were performed with SPINAL64 decoupling during acquisition (7). A phase modulated Lee-Goldberg (PMLG) was used in the PISEMA indirect dimension to decouple proton-proton interactions while allowing for the evolution of $^1H^{-15}N$ DC (8, 9). The initial 90° ^1H pulse, cross-polarization, PMLG (^1H effective field), and SPINAL decoupling during acquisition were applied at ≈60 kHz RF field strength. For SAMPI4 experiments, an RF field strength of 50 kHz was used. Spectra of [U-^{15}N] samples were acquired with 1 k scans and 30 t_1 increments, while selectively labeled samples required 4–12 k scans and ≈8–16 increments. Experiments were performed using both Bruker and Varian spectrometers. The DMX Bruker spectrometer (National High Magnetic Field Laboratory) operating at a ^1H frequency of 600 MHz was equipped with a low-E probe built by the RF program (10). The Varian VNMRS spectrometers operating at ^1H frequencies of 600 and 700 MHz were equipped with a BioStatic probe from Varian, Inc.

χ^1 Rotamers from ^3J Couplings. χ^1 rotamers were determined by measuring $^3J_{C'C\gamma}$ and $^3J_{NC\gamma}$ with quantitative 2D spin echo difference spectroscopy by Bax and coworkers (16). For Thr, Val, and Ile residues $^3J_{C'C\gamma}$ and $^3J_{NC\gamma}$ were measured using 2D experiments described previously (17–19). Aromatic $^3J_{NC\gamma}$ couplings for Phe and Tyr were measured using the pulse sequence described by Hu et al. (20). All of the spectra were acquired using a Varian DirectDrive VNMRS spectrometer operating at ^1H frequency of 600 MHz.

Structural Calculations. The structure calculations were carried out using X-PLOR-NIH software (11) as more completely described in the companion paper (12). We defined a hybrid solution and solid-state NMR target function (E_T), which is formulated as a combination of geometrical (E_{chem}), solution NMR (E_{solNMR}), and solid-state NMR (E_{ssNMR}) terms:

$$E_T = E_{\text{chem}} + E_{\text{solNMR}} + E_{\text{ssNMR}}$$

The potential energy functions (E) are expressed in the form wE, where w represents the relative weight for each energy term, which has been optimized as reported by Shi et al. (12). All of the restraints are approximated by harmonic functions. Specifically, both CSA and DC potentials were implemented as flat-well potential functions according to Bertram and coworkers (13). The experimental errors for CSA and DC were set to 5 ppm and 0.5 kHz, respectively.

The hybrid conformational ensemble was generated starting from AFA-PLN in an extended configuration. In the first stage, we implemented only solution NMR restraints (NOE, torsion angles, and hydrogen bonds). The temperature was decreased from 6000 K to 0 K in steps of 5 K. At each temperature, 20 ps of torsion angle dynamics and several steps of minimization in both torsion angle and Cartesian space were performed. This step folds PLN secondary structure elements. The second structural ensemble was generated by including orientational restraints obtained from PISEMA data. Starting from this folded configuration, solid-state NMR restraints (both CSA and DC) are combined with the solution NMR data into a simulated annealing protocol. To satisfy CSA and DC data, we carried out simulated annealing starting from 3000 K using only torsion angle dynamics. The force constants for the solid-state NMR restraints were optimized using cross-validation (14). To orient PLN with respect to the z direction (corresponding to a fictitious lipid bilayer normal), we used rigid body minimization under orientational restraints with the E_z potential. The depth-dependent potential term (E_z) has been described by DeGrado and coworkers, and is based on the propensity of amino acid residues in a helix to have depth-dependence insertions into the bilayer (15). In the final X-PLOR-NIH refinement protocol, the calculation was performed starting from 300 K using both torsion angle and Cartesian molecular dynamics to relax local geometries and improve the structure quality without significantly changing the orientation of each conformer generated. A total of 500 monomers were generated. 100 conformers displayed no violations and were selected for statistical analysis (Table 1). The full descriptions of the target function and calculation protocols are available in ref. 12.

Molecular Dynamics. The final stage of the structural refinement was carried out using MD simulations in DOPC lipids with the intent of relaxing the PLN structure in an explicit environment that mimics the interactions of PLN within a cell membrane. The information derived from the E_z potential was used to embed conformer #6 from *PDB 2KB7* into a preequilibrated DOPC bilayer. To insert the protein in the bilayer, the overlapping lipids around the protein were deleted. The system was then slowly heated from 10 K to 310 K over 300 ps with the protein harmonically restrained with a force constant of 20 kcal $mol^{-1}Å^{-2}$. The restraints were decreased to 5 kcal $mol^{-1}Å^{-2}$ during heating and maintained for 10 ns of equilibration. Following equilibration, the restraints were removed and the system was further simulated for 100 ns.

The set-up and heating were done using CHARMM Version 33a2 (21), whereas the equilibration and sampling were performed with NAMD version 2.6. The PARAM27 force field with the CMAP correction (22–24) was used throughout the simulation. The system consisted of AFA-PLN (+3 charge), 122 DOPC molecules equally distributed between the top and bottom layer and TIP3P waters. Counter ions were added to achieve electroneutrality and an ionic strength near physiology conditions. Hexagonal periodic boundary conditions were used with a unit cell of 68 × 68 × 88 Å. The particle-mesh-Ewald (PME) method with a mesh of ≈1 Å was used to describe the electrostatic interactions (25). Van der Waals interactions were evaluated using a cutoff scheme feathered to zero between 9 and 11 Å with a switching function. Constant pressure (1 atm) and temperature (310 K) were maintained during MD simulations through Nose-Hoover Langevin piston (26, 27) and Langevin dynamics. The RATTLE algorithm was applied to covalent hydrogen bonds and an integration time step of 2 fs was used.

1. Buck B et al. (2003) Overexpression, purification, and characterization of recombinant ca-ATPase regulators for high-resolution solution and solid-state NMR studies. *Protein Expr Purif* 30:253–261.
2. Vorherr T, Wrzosek A, Chiesi M, Carafoli E (1993) Total synthesis and functional properties of the membrane-intrinsic protein phospholamban. *Protein Sci* 2:339–347.
3. Karim CB, Marquardt CG, Stamm JD, Barany G, Thomas DD (2000) Synthetic null-cysteine phospholamban analogue and the corresponding transmembrane domain inhibit the ca-ATPase. *Biochemistry* 39:10892–10897.
4. Traaseth NJ, Buffy JJ, Zamoon J, Veglia G (2006) Structural dynamics and topology of phospholamban in oriented lipid bilayers using multidimensional solid-state NMR. *Biochemistry* 45:13827–13834.
5. Wu CH, Ramamoorthy A, Opella SJ (1994) High-resolution heteronuclear dipolar solid-state NMR spectroscopy. *J Mag Reson* 109:270–272.
6. Nevzorov AA, Opella SJ (2007) Selective averaging for high-resolution solid-state NMR spectroscopy of aligned samples. *J Magn Reson* 185:59–70.
7. Fung BM, Khitrin AK, Ermolaev K (2000) An improved broadband decoupling sequence for liquid crystals and solids. *J Magn Reson* 142:97–101.
8. Vinogradov E, Madhu PK, Vega S (1999) High-resolution proton solid-state NMR spectroscopy by phase-modulated Lee–Goldburg experiment. *Chem Phys Lett* 314:443–450.
9. Fung BM, Ermolaev K, Yu Y (1999) ^{13}C NMR of liquid crystals with different proton homonuclear dipolar decoupling methods. *J Mag Reson* 138, 28–35.
10. Gor'kov PL, et al. (2007) Using low-E resonators to reduce RF heating in biological samples for static solid-state NMR up to 900 MHz. *J Magn Reson* 185:77–93.
11. Schwieters CD, Kuszewski JJ, Tjandra N, Clore GM (2003) The xplor-NIH NMR molecular structure determination package. *J Magn Reson* 160:65–73.
12. Shi L, et al. (2009) A refinement protocol to determine the structure, topology, and depth of insertion of membrane proteins using hybrid solution and solid-state restraints. *J Biomolec NMR*, in press.
13. Bertram R, et al. (2003) Atomic refinement with correlated solid-state NMR restraints. *J Magn Reson* 163:300–309.
14. Kim S, Quine JR, Cross TA (2001) Complete cross-validation and R-factor calculation of a solid-state NMR derived structure. *J Am Chem Soc* 123:7292–7298.
15. Senes A, et al. (2007) E(z), a depth-dependent potential for assessing the energies of insertion of amino acid side-chains into membranes: Derivation and applications to determining the orientation of transmembrane and interfacial helices. *J Mol Biol* 366:436–448.
16. Bax A, et al. (1994) Measurement of homo- and heteronuclear J couplings from quantitative J correlation. *Methods Enzymol* 239:79–105.
17. Hu JS, Bax A (1997) Chi 1 angle information from a simple two-dimensional NMR experiment that identifies trans 3JNC gamma couplings in isotopically enriched proteins. *J Biomol NMR* 9:323–328.
18. Grzesiek S, Vuister GW, Bax A (1993) A simple and sensitive experiment for measurement of JCC couplings between backbone carbonyl and methyl carbons in isotopically enriched proteins. *J Biomol NMR* 3:487–493.
19. Vuister GW, Wang AC, Bax A (1993) Measurement of three-bond nitrogen-carbon J couplings in proteins uniformly enriched in 15N and 13C. *J Am Chem Soc* 115:5334–5335.
20. Hu JS, Grzesiek S, Bax A (1997) Two-dimensional NMR methods for determining Chi1 angles of aromatic residues in proteins from three-bond JC'cg and JNCg couplings. *J Am Chem Soc* 119:1803–1804.
21. Brooks BR, et al. (1983) CHARMM: A program for macromolecular energy, minimization, and dynamics calculations. *J Comp Chem* 4:187–217.
22. MacKerell AD, et al. (1998) All-atom empircal potential for molecular modeling and dynamics studies of proteins. *J Phys Chem B* 102:3586–3516.
23. Mackerell AD, Jr, Feig M, Brooks CL, 3rd (2004) Extending the treatment of backbone energetics in protein force fields: Limitations of gas-phase quantum mechanics in reproducing protein conformational distributions in molecular dynamics simulations. *J Comput Chem* 25:1400–1415.
24. Mackerell AD, Jr (2004) Empirical force fields for biological macromolecules: Overview and issues. *J Comput Chem* 25:1584–1604.
25. Ewald P (1921) Die Berechnung optischer und elektrostatischer Gitterpotentiale. *Ann Phys* 369:253–287.
26. Martyna GJ, Tobias DJ, Klein ML (1994) Constant pressure molecular dynamics algorithms. *J Chem Phys* 101:4177–4189.
27. Feller SE, Zhang Y, Pastor RW, Brooks BR (1995) Constant pressure molecular dynamics simulation: The Langevin piston method. *J Chem Phys* 103:4613–21.

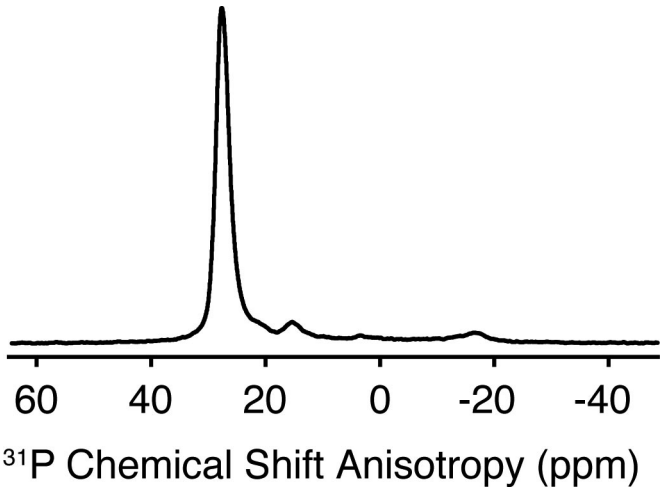

Fig. S1. ^{31}P spectrum of the [U-^{15}N] AFA-PLN sample in Fig. 1*C*. A single-pulse on ^{31}P was acquired with proton decoupling to verify the alignment of the lipid bilayer. This spectrum is representative of the selectively labeled samples shown in Fig. 1.

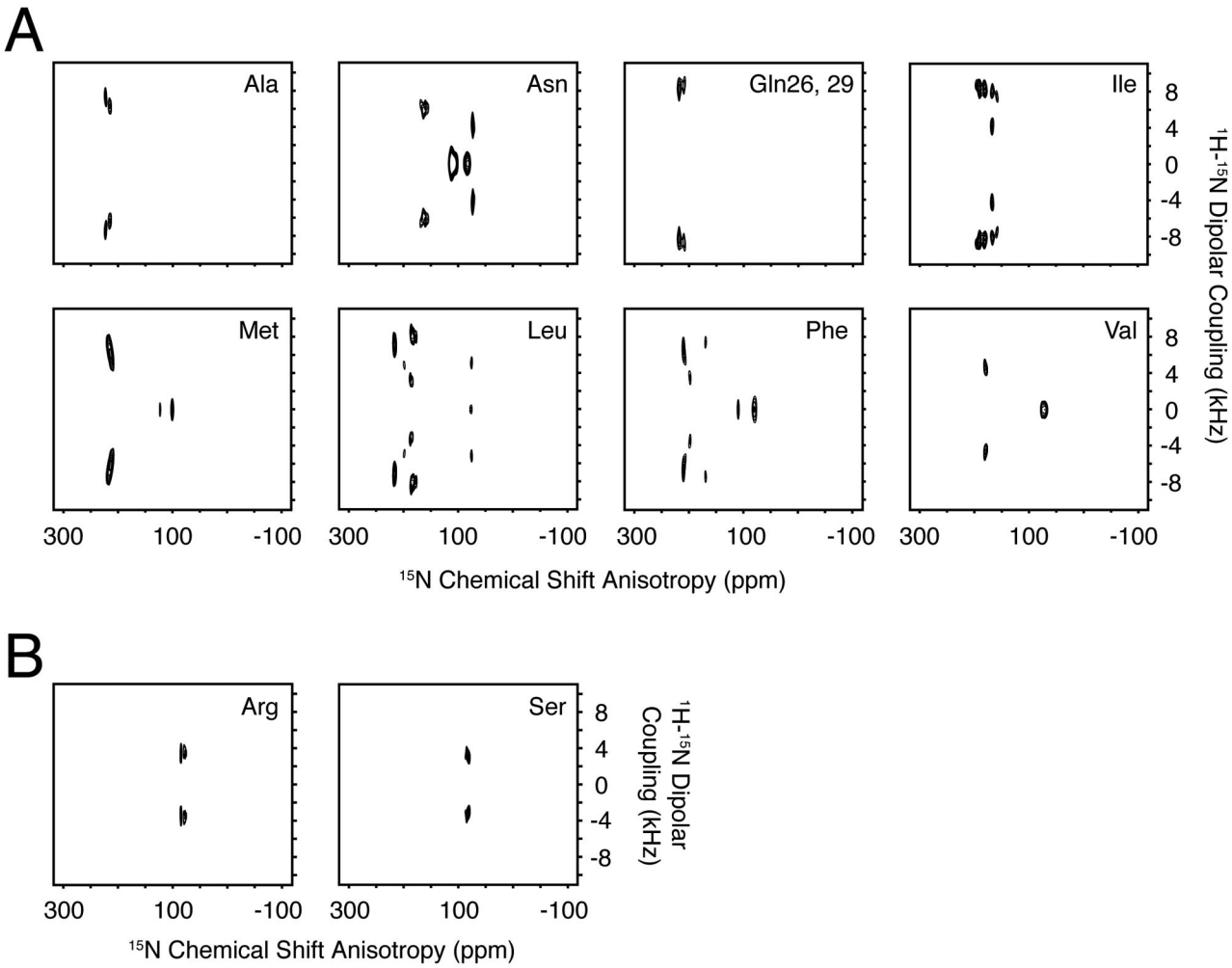

Fig. S2. Supplement to Fig. 1 showing full PISEMA spectra. Note that the Asn and Phe spectra show resonances upfield of those plotted in Fig. 1 due to the side chain ^{15}N resonances of Asn (the HSQC of the Phe sample showed scrambling to ^{15}N Asn side chains). Due to the RF offsets (^{15}N - 200 ppm, ^{1}H - 5–6 ppm), some of the cytoplasmic domain peaks in the 2D PISEMA spectra (*A*) show up with 1) lower intensity than the peaks in domain Ib and II or 2) at zero-frequency indicating that those residues have an amide proton off-resonance from that used in the experiment. For several cytoplasmic domain resonances, SAMPI4 experiments (*B*) were run to obtain these frequencies (CSA and DC) more accurately.

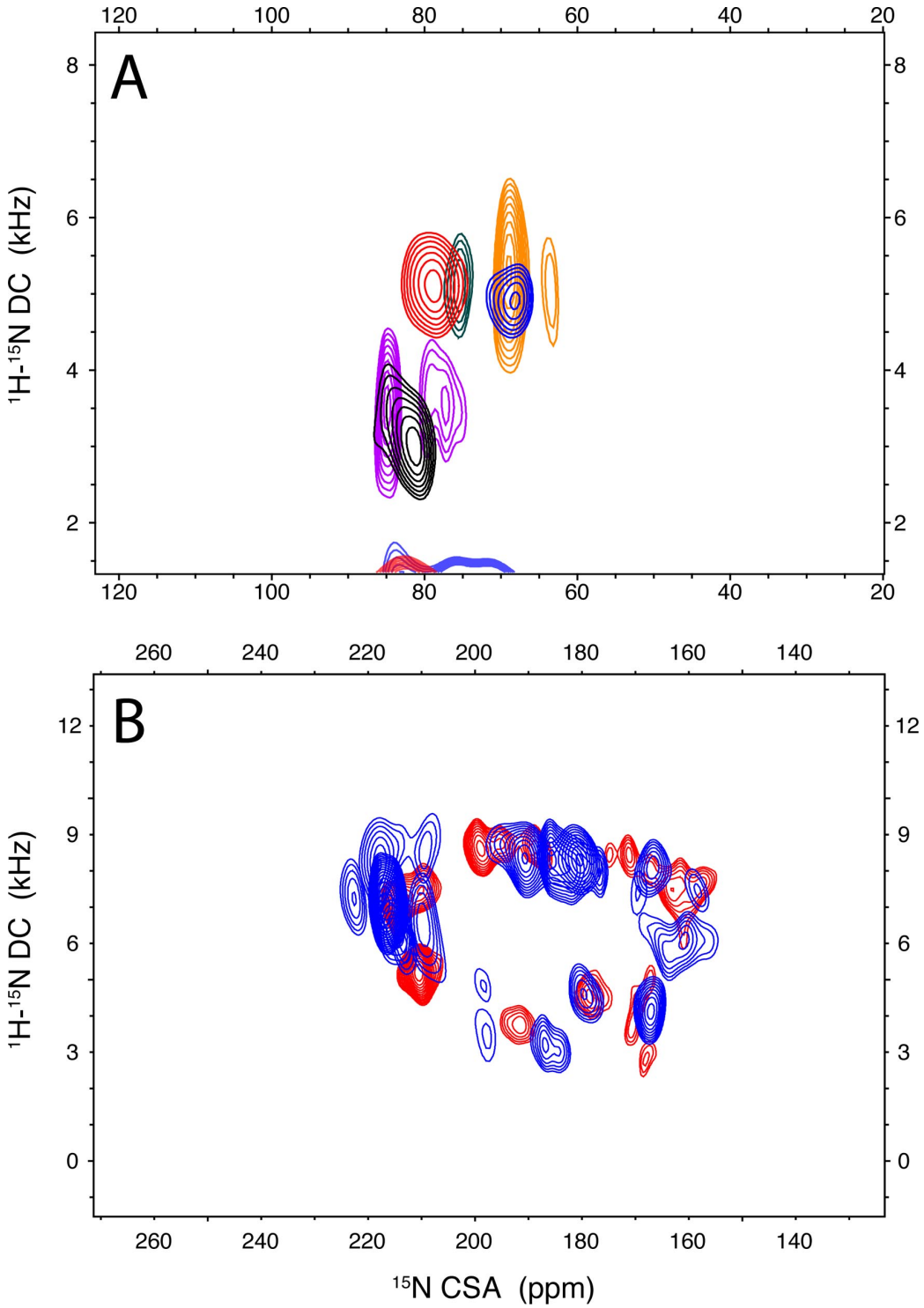

Fig. S3. Overlay of spectra for domain Ia (*A*) and domain Ib and II (*B*). *A* is color-coded with residue-type: orange-[^{15}N-Ala], red-[^{15}N-Thr], blue-[^{15}N-Val], purple-[$^{15}N_{\alpha}$-Arg], light blue-[^{15}N-Leu], and black-[^{15}N-Ser]. The Arg and Ser spectra were acquired using the SAMPI4 pulse sequence, while all others were acquired using the PISEMA experiment. The appearance of zero-frequency peaks in the spectra of [^{15}N-Val] and [^{15}N-Thr] are due to a mismatched ^{1}H-offset. *B* is an overlay of all selectively labeled PISEMA spectra shown in Fig. 1*D* (blue) with the [U-^{15}N] spectrum equilibrated in D_2O (red). The small changes between these spectra arise from peaks missing in the [U-^{15}N] spectrum due to D_2O exchange, as well as slight differences in CSA and DC in sample-to-sample preparations. Error bars in the CSA and DC restraints reflect the effects.

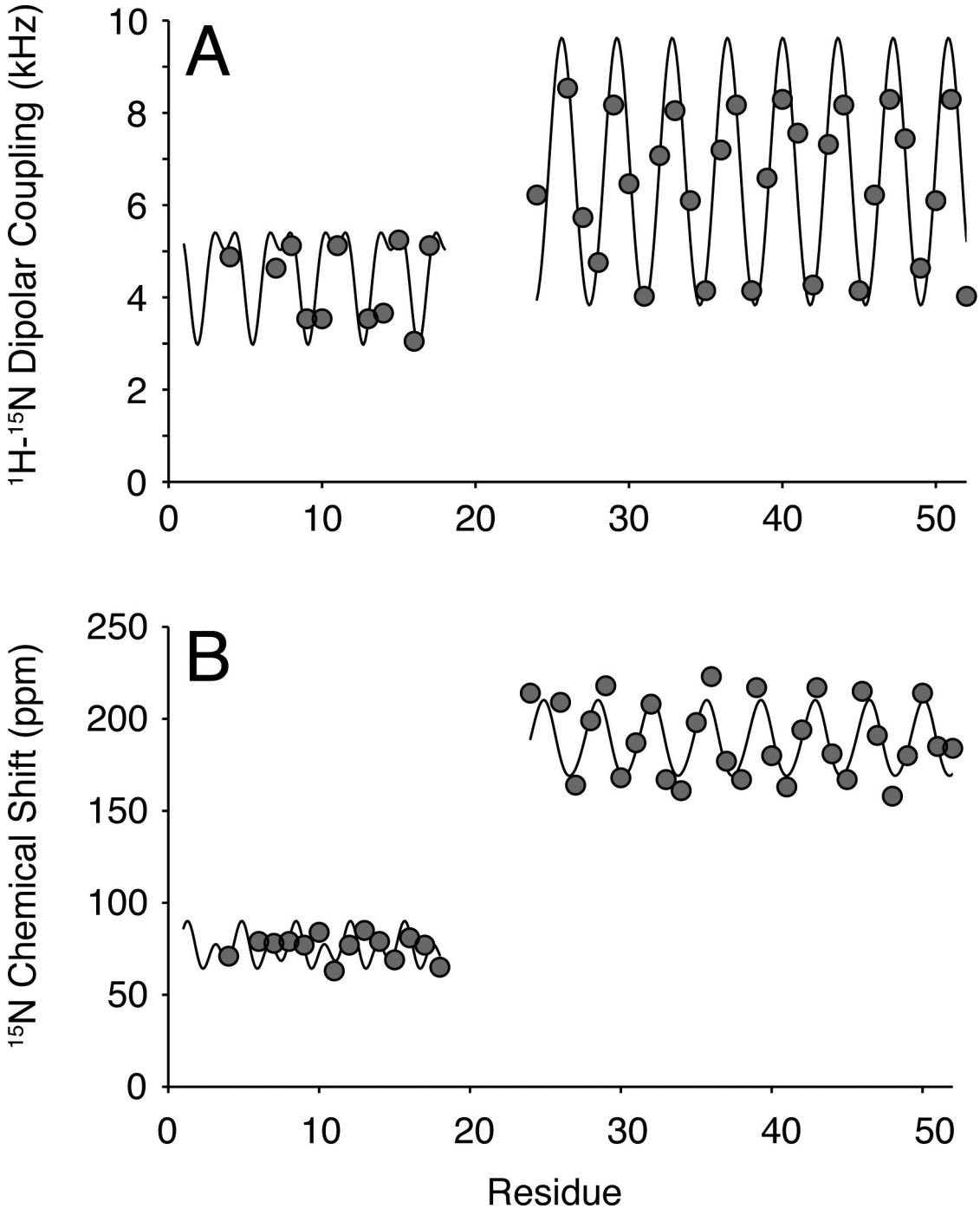

Fig. S4. Supplement to Fig. 2. Data shown are the same as in Fig. 2 *A* and *C*, except with ideal waves plotted with the experimental CSA and DC data.

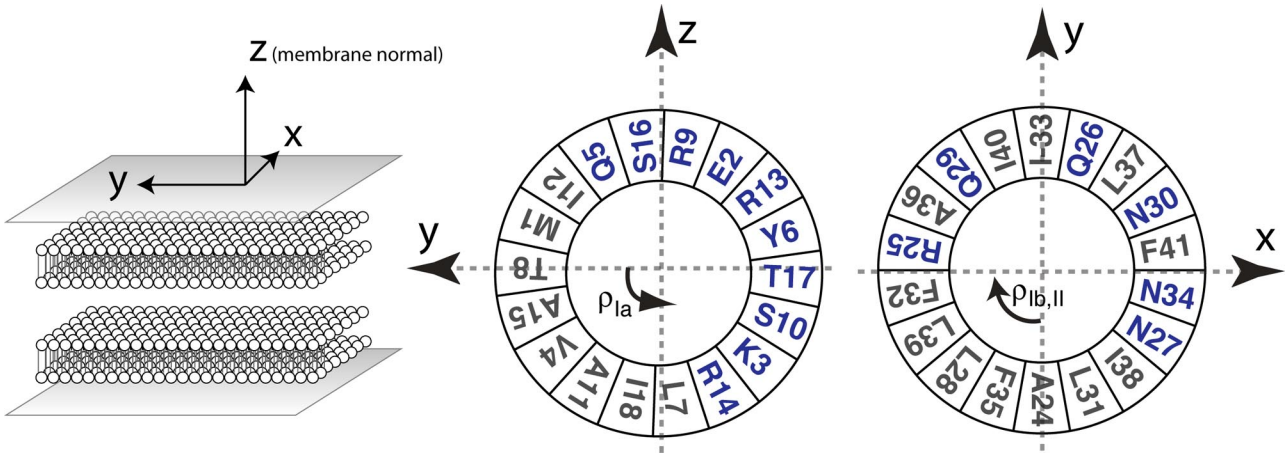

Fig. S5. Description of the angles used in Fig. 3. For the domain Ia rotation angle, ρ_{Ia} is defined to be zero when the vector described by the amide nitrogen of Thr-8 and the center of the helical axis is colinear with the *y* axis. Likewise the $\rho_{Ib,II}$ is similar, with the exception that the amide nitrogen of Ala-24 is used.

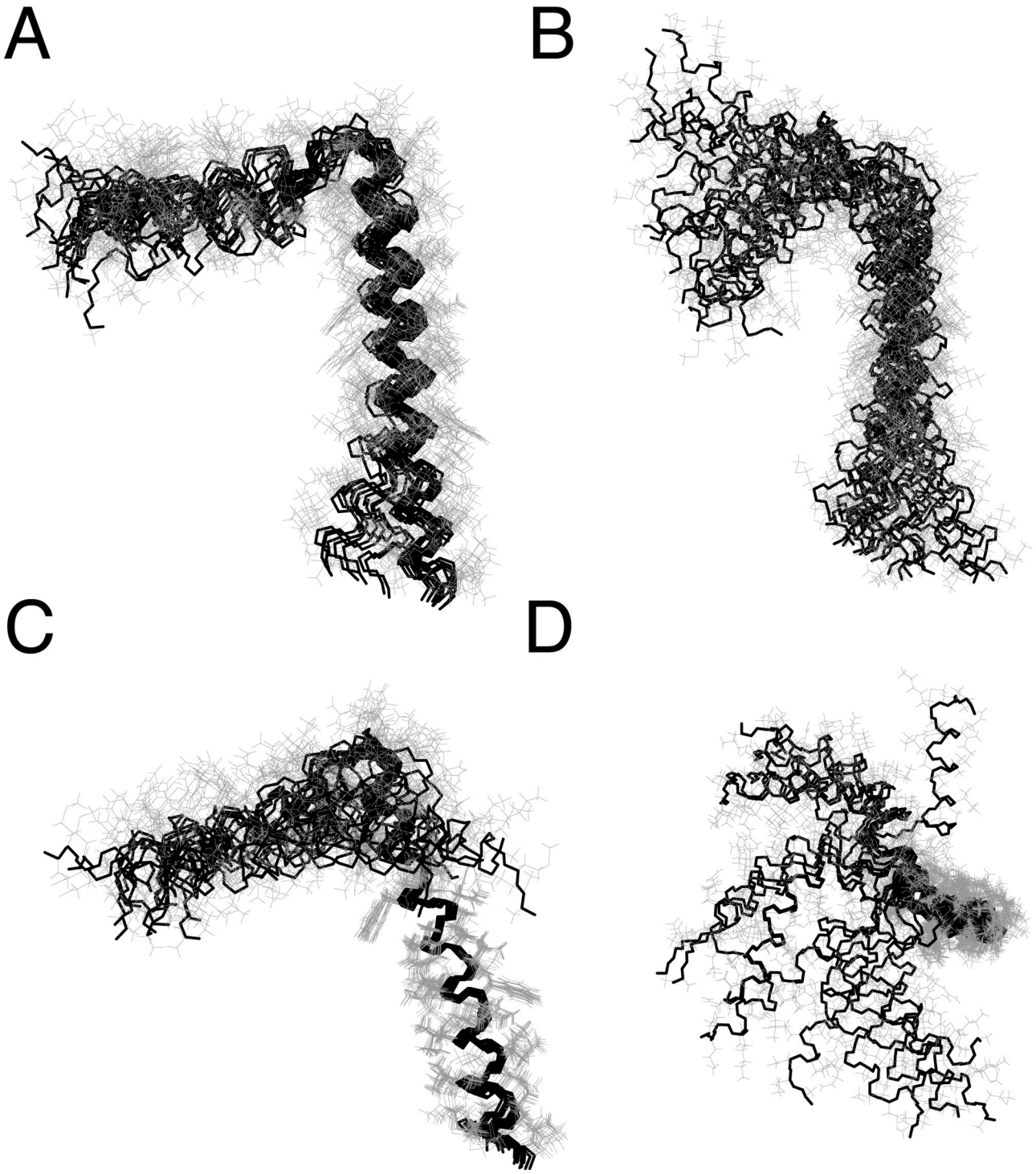

Fig. S6. Ensemble overlay of residues 4–50 for the hybrid (*A*) and solution NMR ensembles (*B*). *C* and *D* show side and top views of the hybrid ensemble where residues 24–50 in domain Ib and II are superimposed.

Table S1. Summary of the NMR restraints from solid-state NMR

Residue	^{15}N CSA (ppm)	^{1}H-^{15}N DC (kHz)
1	101/123	0
4	71	4.9
6	79	
7	78	4.6
8	79	5.1
9	77	3.5
10	84	3.5
11	63	5.1
12	77	
13	85	3.5
14	79	3.7
15	69	5.2
16	81	3.0
17	77	5.1
18	65	
20	101/123	0
24	214	6.2
26	209	8.5
27	164	5.7
28	199	4.8
29	218	8.2
30	168	6.5
31	187	4.0
32	208	7.1
33	167	8.0
34	161	6.1
35	198	4.1
36	223	7.2
37	177	8.2
38	167	4.1
39	217	6.6
40	180	8.3
41	163	7.6
42	194	4.3
43	217	7.3
44	181	8.2
45	167	4.1
46	215	6.2
47	191	8.3
48	158	7.4
49	180	4.6
50	214	6.1
51	185	8.3
52	184	4.0

Note Met1 and Met20 cannot be distinguished in the combinatorial assignment algorithm.

Table S2. Summary of $\chi 1$ restraints used in the hybrid calculation

Residue	χ^1
4	180
6	180
7	−60
17	60
28	−60
31	−60
32	180
33	−60
35	180
41	180
43	−60
44	−60
45	−60
47	−60
48	−60
49	180

Table S3. Summary of synthetic or bio-expressed AFA-PLN samples used for solid-state NMR experiments

AFA-PLN Label	Synthetic or Bio-expressed PLN
[^{15}N-Ala]	Bio
[^{15}N-Arg]	Bio
[^{15}N-Asn]	Bio
[^{15}N-Ile]	Bio
[^{15}N-Met]	Bio
[^{15}N-Leu]	Bio
[^{15}N-Phe]	Bio
[^{15}N-Val]	Bio
[^{15}N-Ser]	Synthetic
[$^{15}N_{\alpha}$-Gln26, Gln29]	Synthetic